Continental Shelf Research, Vol. 11, Nos 8–10, pp. 1181–1197, 1991
Printed in Great Britain.

0278–4343/91 $3.00 + 0.00

Interaction of internal waves with the seabed on continental shelves

B. BOCZAR-KARAKIEWICZ,* J. L. BONA† and B. PELCHAT‡

(*Received* 22 *January* 1990; *in revised form* 16 *August* 1990; *accepted* 6 *December* 1990)

Abstract—Large-amplitude internal waves generated by tidal fluctuations at the outer edge of the continental shelf propagate shoreward and interact with seabed sediment. A crude mathematical model describing the propagation of such internal waves is used to predict wave-induced sediment flux and thereby to provide a possible explanation of sand-ridge formation on continental shelves. The ocean over the shelf is modelled as a two-layer system and it is assumed that the internal waves are generated at the shelf edge. Field measurements indicate that the very low frequency tidal fluctuations create a train of internal oscillations of periods between 15 and 20 min. Because of nonlinear effects these wave trains generate differential sediment fluxes and, in the model, this leads to the creation of seabed topography. The predictions of the model are tested against field data collected on the eastern Canadian continental shelf and in particular on Sable Island Bank and the Grand Banks of Newfoundland. The comparisons between predictions and measurements are encouraging especially in light of the fact that the model has no free parameters.

INTRODUCTION

LONG-crested sand ridges with successive crest-to-crest distances of hundreds to thousands of metres are known to form on continental shelves (SWIFT and FREELAND, 1978; FIELD, 1980; SWIFT *et al.*, 1972; AMOS and KING, 1984; FIELD and ROY, 1984; HOOGENDOORN and DALRYMPLE, 1986; MARTIN and FLEMMING, 1986). Of particular interest here are sandy bedforms whose spacing to depth ratio is intermediate between the order one ratio corresponding to the sand waves described by RICHARDS (1980) and the order 10^{-2} ratio corresponding to tidal ridges described by HUTHNANCE (1982). The theories presented in these papers appear not to account for the sand ridges that are the focus of attention here. The stability of these sand ridges suggests that they may be time-averaged responses to the hydrodynamics of their environment. Consideration of the large scales involved indicates that locally-generated storm waves are not a likely candidate as the progenator of such structures (DUANE *et al.*, 1972). Currents induced by atmospheric forcing and by the local barotropic tide appear only to modify the existing ridges without contributing essentially to their formation and to their main morphological features (AMOS *et al.*, 1988).

In earlier work (BOCZAR-KARAKIEWICZ and BONA, 1986; BOCZAR-KARAKIEWICZ *et al.*, 1990) a mechanism associated with surface waves in the infragravity range (waves with periods of 0.5–5 min) that may account for fields of sand ridges was proposed. These long-

* Université du Québec, INRS-Oceanologie, Québec, Canada.
† Department of Mathematics, Pennsylvania State University, University Park, PA 16802, U.S.A.
‡ Institut Maurice-Lamontagne, Mont-Joli, Québec, Canada.

period waves span the gap in the frequency spectrum between ordinary gravity waves and tidal oscillations. In general their origin has been loosely linked with wind, very large storm systems, and underwater seismic activity (KINSMAN, 1965). In the present work a second mechanism associated with large-amplitude internal waves is shown to have potential for transporting near-bed sediment and so for forming large-scale structures in the seabed.

Internal waves are frequently observed in stratified waters on the continental shelf. They appear as highly-coherent groups having a well-defined wavelength and they propagate shoreward with crests oriented generally along isobaths (APEL, 1979, 1980; APEL and GONZALES, 1983; BAINES, 1981; SANDSTRÖM and ELLIOTT, 1984; HOLLOWAY, 1987; SANDSTRÖM *et al.*, 1989). The average length of these waves is on the order of 400 m (with a range of 200–1600 m depending on the location) which is often considerably larger than the water depth above the shelf. These waves appear to result from the disintegration of internal tides as they propagate shoreward from the deep ocean and encounter the continental shelf (MAXWORTHY, 1979; HOLLOWAY, 1987; HEATHERSHAW *et al.*, 1987). Various hydrodynamical aspects of internal waves on continental shelves have attracted attention. The resulting work concerns the generation, propagation, sloping, and breaking of internal waves (DJORDJEVIC and REDEKOPP, 1978; HELFRICH *et al.*, 1984; KAO *et al.*, 1985; HELFRICH and MELVILLE, 1986; WALLACE and WILKINSON, 1988; IVEY and NOKES, 1989). Observations indicate that the near-bed motions induced by these waves are sufficiently energetic to lift and transport loose sediment (SOUTHARD and CACCHIONE, 1972; CACCHIONE and SOUTHARD, 1974; SANDSTRÖM and ELLIOTT, 1984; KARL *et al.*, 1986; STEWART, 1986).

This paper describes a mechanism of wave-bed interaction induced by internal waves. The associated mathematical model provides predictions about the near-bed sediment flux and about the formation of large-scale sand ridges. Results obtained from the model are compared with data from the Scotian Shelf, Sable Island Bank (SANDSTRÖM and ELLIOTT, 1984; HOOGENDOORN and DALRYMPLE, 1986; AMOS and NADEAU, 1988) and from the Grand Banks of Newfoundland (FADER and KING, 1981; BARRIE *et al.*, 1984). Predictions are also compared with observations of sand ridges on the continental platform of Australia (FIELD and ROY, 1984) and Africa (MARTIN and FLEMMING, 1986).

THE MODEL

The proposed model has four constituent processes describing wave-bed interactions, namely: (1) the hydrodynamics of the main water body; (2) the near-bed boundary-layer flow; (3) sediment transport; and (4) evolution of bed topography. These four modules are linked together and the resulting model is discretized for numerical integration. The integration consists of a two-step procedure. In the first step the fluid flow and the sediment flux are calculated over a bed configuration that is fixed. In the second step the temporal evolution of the seabed is calculated while keeping all variables describing the fluid and sediment flow constant. This two-step approximation is justified both on mathematical grounds and by observations in laboratory and natural shelf environments that indicate significant changes in bed topography occur only over a period of many thousands of wave periods. This time-scale is quite long when compared to the rapid changes in the fluid flow that occur during one wave period. (BOCZAR-KARAKIEWICZ *et al.*, 1987; BOCZAR-KARAKIEWICZ *et al.*, 1990).

The hydrodynamics of the main water body

The proposed model describes the evolution of long-period internal oscillations over a gently sloping seabed using nonlinear, dispersive, shallow-water theory. The waves are assumed to propagate through a simplified medium consisting of an inviscid, two-layer fluid system which at rest comprises a lighter fluid of density ρ_1, bounded by a rigid upper surface resting on a heavier fluid of density ρ_2 which is bounded below by the seabed (Fig. 1). In this idealized version of the bed–fluid system it is assumed that the incident internal waves propagate shoreward from the shelf edge and that the incoming wave train is of constant amplitude and frequency. At the present stage of modeliing it is assumed that the internal waves and the shelf topography do not vary appreciably in the longshore direction so that both the wave and bed motion are two-dimensional. In Fig. 1, $\bar{x}$ is the horizontal coordinate with $\bar{x} = 0$ at the shelf edge, $\bar{z}$ is the vertical coordinate with $\bar{z} = 0$ at the equilibrium position of the interface, and $\bar{\zeta} = \bar{\zeta}(\bar{x}, \bar{t})$ is the deviation of the interface from its equilibrium position $\bar{z} = 0$ at the point $\bar{x}$ at time $\bar{t}$. The characteristic depth of the water at the edge of the shelf is denoted by H, while h_1 and h_2 are the characteristic depths of the two layers at $\bar{x} = 0$. The local depth of the lower fluid layer is written as $\bar{h}(\bar{x})$.

The governing equations based on the assumptions of incompressible, inviscid flow (except at the interface across which the flow may be discontinuous) and continuity of pressure across the interface, are then

$$\Delta\bar{\Phi} = 0 \quad \text{for} \quad \bar{z} \neq \bar{\zeta} \tag{1.1}$$

$$\bar{\Phi}_{\bar{z}} = 0 \quad \text{at} \quad \bar{z} = h_1 \tag{1.2}$$

$$\bar{\Phi}_{\bar{z}} = \bar{\Phi}_{\bar{x}}\bar{h}_{\bar{x}} \quad \text{at} \quad \bar{z} = -h, \tag{1.3}$$

$$\bar{\Phi}_{\bar{z}} = \bar{\zeta}_{\bar{t}} + \bar{\Phi}_{\bar{x}}\bar{\zeta}_{\bar{x}} \quad \text{at} \quad \bar{z} = \bar{\zeta}_{\pm}, \quad \text{and} \tag{1.4}$$

$$\rho_1[g\bar{\zeta} + \bar{\Phi}_{\bar{t}} + \tfrac{1}{2}(\nabla\bar{\Phi})^2]_{\bar{z}=\bar{\zeta}_+} = \rho_2\{g\bar{\zeta} + \bar{\Phi}_{\bar{t}} + \tfrac{1}{2}(\nabla\bar{\Phi})^2\}_{\bar{z}=\bar{\zeta}_-}. \tag{1.5}$$

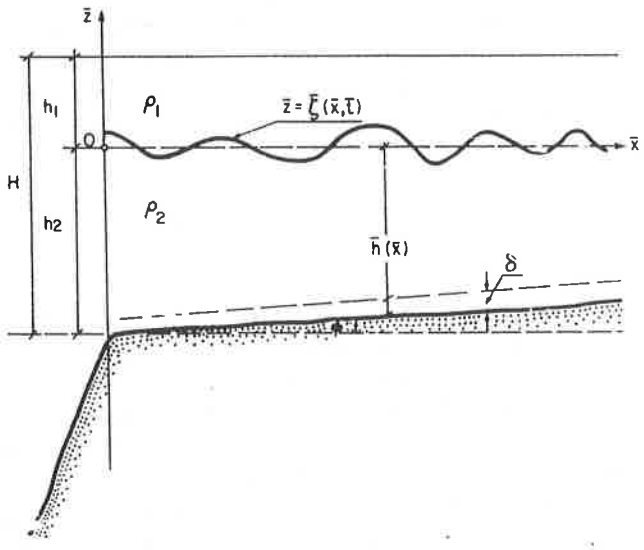

Fig. 1. The configuration of the two-layer fluid system

where $\bar{\Phi}(\bar{x}, \bar{z}, \bar{t})$ is the velocity potential of the flow. The subscripts $\bar{x}$, $\bar{z}$, $\bar{t}$ signify partial differentiation with respect to the indicated variable. Here and subsequently the evaluation of a variable at $\bar{z} = \bar{\zeta}_+$ is at a value of $\bar{z}$ slightly larger than $\bar{\zeta}$ where the limit is taken as $\bar{z}$ tends to $\bar{\zeta}$ from above, with the obvious modification for evaluation at $z = \zeta_-$.

We consider here solutions of equations (1) that correspond to small-amplitude waves in a two-layer fluid of gradually varying total depth. The significant dimensionless parameters are

$$\beta = \frac{\bar{h}}{\bar{\lambda}}, \qquad \alpha = \frac{a}{\bar{h}}, \qquad \kappa = \frac{\rho_2 - \rho_1}{\rho_2 + \rho_1}, \qquad \text{and} \qquad \varepsilon = \frac{\bar{\lambda}}{\bar{\lambda}_h}, \tag{2}$$

where $\bar{\lambda}$ is a characteristic length of the waves in question, $\bar{h}$ is a characteristic water depth, a is a characteristic amplitude (which may be either positive or negative) and $\bar{\lambda}_h$ is a characteristic length for the depth variation. The parameters α, β, κ and ε are small by hypothesis and, following KELLER (1988), we treat β as the basic perturbation parameter.

Scaled, non-dimensional variables are derived as follows:

$$(x, z) = \frac{1}{h_2}(\bar{x}, \bar{z}), \qquad t = \left(\frac{g}{h_2}\right)^{1/2} \bar{t}, \qquad \beta\zeta(X, x, z, t) = \frac{1}{h_2}\bar{\zeta}(\bar{x}, \bar{z}, \bar{t}),$$

$$\beta\Phi(X, x, z, t) = \frac{1}{h_2(gh_2)^{1/2}}\bar{\Phi}(\bar{x}, \bar{z}, \bar{t}), \qquad X = \beta x.$$

The first step is to expand the interfacial variable ζ and the velocity potentials $\Phi_\pm$ in powers of β, as $\zeta = \zeta^{(1)} + \beta\zeta^{(2)} + \ldots$, $\Phi_\pm = \Phi_\pm^{(1)} + \beta\Phi_\pm^{(2)} + \ldots$. Substituting these expansions into the non-dimensional versions of equations (1.1)–(1.5) and equating like powers of β leads to an infinite system of equations. The variation in the variable z and the velocity potentials can be systematically eliminated in a standard way to leave a collection of coupled Boussinesq-type equations for $\zeta^{(1)}, \zeta^{(2)}, \ldots$ [see the Appendix, equations (A1) and (A2)]. At this stage the assumptions are the same as those that lead to any of the Korteweg–de Vries or Boussinesq theories for internal waves (cf. BENNEY, 1966; or TURNER, 1973). The description of the interfacial motion is further simplified by seeking a solution for which the first approximation $\zeta^{(1)}$ to the interface ζ is represented approximately by the simple modal decomposition

$$\zeta^{(1)}(X, x, t) = \sum_{j=1}^{2} a_j(X) \exp\left[i(k_j x - \omega_j t)\right] + \text{c.c.} \tag{3}$$

Here ω_1 is the frequency of the postulated incoming train of internal oscillations and $\omega_2 = 2\omega_1$ is its second harmonic, while k_1 and k_2 are the wave numbers associated with ω_1 and ω_2, respectively. The length scale λ associated with the wavetrain is taken to be $\lambda = \lambda_1 = 2\pi/k_1$. [Note that the decomposition in (3) explicitly disregards the possibility of reflected waves. Such waves can be accommodated within this model but for reasons of simplicity they have not been considered. The laboratory observations of MAHONY and PRITCHARD (1980) and WALLACE and WILKINSON (1988) and field observations of APEL *et al.* (1975) indicate that reflection is not a major factor over the sort of gentle slopes that typify the regions of study.] It will turn out that the relationship between ω_j and k_j, $j = 1,2$, is determined by the dispersion relation arising from linearized, gravity-wave theory. The

first-order complex amplitudes in (3) are taken to vary on the scale of wavelengths and, therefore to depend only on the long scale X. In equation (3) c.c. stands for the complex conjugate of the quantity just preceding it. The first approximation to the velocity potentials corresponding to (3) has the form

$$\Phi_{\pm}^{(1)}(X, x, z, t) = -\sum_{j=1}^{2}\left[i\frac{a_j(X)}{\omega_j}\exp\left[i(k_j x - \omega_j t)\right]\frac{\cosh\left(k_j(z+h)\right)}{\cosh\left(k_j h\right)} + \text{c.c.}\right]. \tag{4}$$

The presumption that the principal features of the bottom variation are gradual and that their amplitude ε is small means that it is assumed that $h = h(X)$ is also a function only of the long variable X.

When the assumed expansion (3) for $\zeta^{(1)}$ is substituted into the first of the system of Boussinesq equations one obtains a linearized dispersion relation between the frequencies ω_j and wavenumbers k_j, $j = 1$ and 2 namely

$$k_j = \omega_j\left(\frac{H}{\rho h_1}\right)^{1/2}\left(1 + \frac{1}{3}\frac{H}{\rho h_2}\omega_j^2\right)^{1/2} \tag{5}$$

where $\rho = (\rho_2 - \rho_1)/\rho_2$. With k_1 and k_2 determined, one then proceeds to the next Boussinesq equation. At this stage a second approximation $\zeta^{(2)}$ in (3) yields equations for the complex amplitudes a_1 and a_2, namely

$$\begin{aligned} a_1' &= \frac{\varepsilon}{\beta} f H_1 a_1 + i\frac{\alpha}{\beta} S_1 \exp\left[-i\frac{\Delta k}{\beta} X\right] a_1^* a_2 \\ a_2' &= \frac{\varepsilon}{\beta} f H_2 a_2 + i\frac{\alpha}{\beta} S_2 \exp\left[i\frac{\Delta k}{\beta} X\right] a_1^2, \end{aligned} \tag{6}$$

where the prime signifies differentiation with respect to X (see Appendix). These equations comprise a coupled system of first-order, ordinary differential equations where H_1, H_2, S_1, and S_2 are functions of X determined by the wave parameters ω_j and k_j where $j = 1$ and 2, and by the geometric and constitutive parameters h_1, h_2, H and ρ which characterize the two-layer fluid system. The influence of the bed topography is expressed in the first terms on the right-hand side of (6) because f is given in terms of $h(X)$. Precise definitions of the quantities f, H_1, H_2, S_1 and S_2 are presented in the Appendix.

Equations (5) and (6) must be supplemented by the frequency ω_1 of the incident wave, by the incident wave energy (a_1 and a_2 at $X = 0$), and by a bed topography $h(x) = \tilde{h}(\bar{x})/h_2$ (which is instantaneously fixed but which will be successively updated by the calculation carried out in the fourth stage of the model).

Evidence in favour of the wave description used here is provided by laboratory experiments (Wallace and Wilkinson, 1988), by field observations of spectra of internal waves (Hall and Pao, 1969) and by time series of wave-induced currents (Holloway, 1987).

Near-bed boundary-layer flow and resulting sediment transport

The near-bed velocities induced by the internal wave are assumed to drive a sediment-laden, boundary-layer flow over a rippled bed composed of non-cohesive sediment. The

principal horizontal component of the fluid velocity, u, in the bed boundary layer (LONGUET-HIGGINS, 1953; JOHNS, 1970; JACOBS, 1984) may be decomposed into the form

$$u = u^{(1)} + u^{(2)} + U_m \tag{7}$$

where $u^{(1)}$ and $u^{(2)}$ denote the first-order and second-order orbital velocities and U_m represents the time-averaged, mass-transport velocity.

The sediment concentration over a rippled bed has been obtained by solving the advection–diffusion equation (HUNT, 1954) with a near-bed sediment flux given by a model pick-up function (NIELSEN, 1988). The sediment concentration, C, may also be decomposed into components as

$$C = \bar{C}(x, y, z) + \hat{C}(x, y, z, t) \tag{8}$$

where $\bar{C}$ and $\hat{C}$ represent, respectively, the time-independent and the time-dependent contribution to the resultant sediment concentration, C. The description of the boundary flow is validated by the results of numerical experiments using a second-order turbulent closure model (VILLARET and SHENG, 1988). Derivations and explicit expressions for u and C are presented by CHAPALAIN (1988) and CHAPALAIN and BOCZAR-KARAKIEWICZ (1989).

The wave-induced, time-averaged, sediment flux, Q, across the near-bed boundary layer is given by

$$Q = \frac{1}{T}\int_0^T \int_{-h(x)}^{-h(x)+\delta} uC \, dz \, dt = Q_m + Q_t, \tag{9}$$

where δ denotes the boundary-layer thickness and T is the wave period. On the right-hand side of (9) Q_m and Q_t denote, respectively, the contributions of the time-independent and time-dependent components of Q derived from u in (7) and C in (8).

Numerical experiments with a set of typical incident wave characteristics and sediment parameters carried out over sloping bed configurations have shown that the leading order contribution to the sediment flux, Q, is that of Q_m where

$$Q_m = \frac{1}{T}\int_0^T \int_{-h(x)}^{-h(x)+\delta} U_m \bar{C}_0 \exp(Dz) \, dz \, dt, \tag{10}$$

and where U_m is the mass transport velocity introduced in (7), $\bar{C}_0$ is a constant sediment concentration (NIELSEN, 1988), and D is a constant which includes the parameter of diffusivity. The sediment flux Q_m in a two-layer system is directed offshore. By contrast the contribution of the oscillatory components of u and C provide an onshore sediment flux which increases with increasing wave asymmetry (CHAPALAIN, 1988; CHAPALAIN and BOCZAR-KARAKIEWICZ, 1989).

Evolution of the bed topography

The temporal evolution, $\partial h/\partial \tau$, of the bed is related by conservation of mass to spatial variation in the sediment flux via the conservation law

$$\partial h/\partial \tau = \partial Q_m/\partial X \tag{11}$$

where τ is a temporal variable whose scale is slower by several orders of magnitude than the temporal variable t which is measured in wave periods. This modelling presumption is

based on observations which show that vertical changes in sand-ridge morphology are of the order of tens of millimetres per year (HOOGENDOORN and DALRYMPLE, 1986; AMOS and NADEAU, 1988).

The resulting morphological model comprises a set of nonlinear differential equations given by (6) and (11) which have to be supplemented by incident wave characteristics, by an initial bed topography, h_0, and various sediment parameters.

PREDICTIONS AND COMPARISONS

In this section we will present numerical approximations of solutions of the model and compare the resulting predictions with measured bathymetries from two continental shelves: the Grand Banks of Newfoundland and Sable Island Bank. The bed topographies in both regions feature typical arrays of sand ridges.

For the Grand Banks of Newfoundland it is assumed that the nonlinear internal oscillations radiate from the eastern shelf break and that they continue to propagate in a direction normal to the shelf-break (Fig. 2). For Sable Island Bank the model is applied along a shelf transect, that runs approximately normal to the offshore sand ridge field south of Sable Island (Fig. 3). Such a choice assumes that the internal tide and

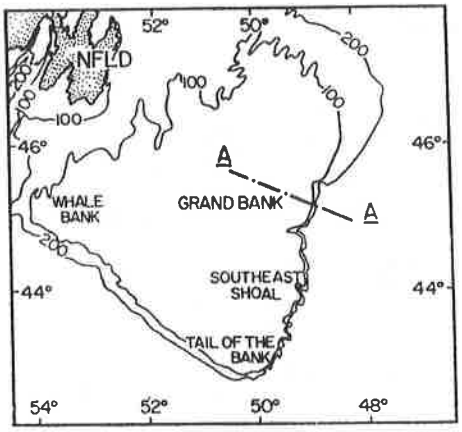

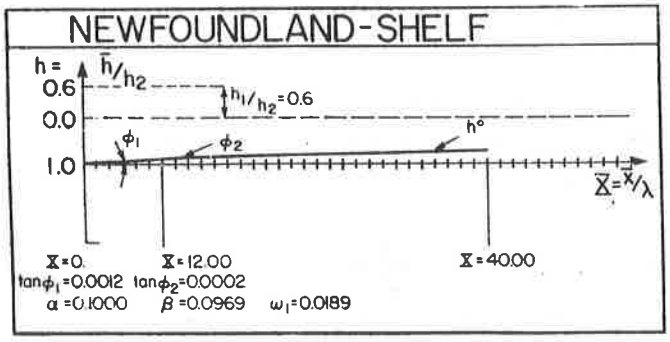

Fig. 2. A location diagram showing the initial seabed and incident wave and stratification parameters applied in the calculation for the Grand Banks of Newfoundland.

consequently the internal wave train approaches the shelf edge from the east-southeast. This agrees with data for the barotropic tide (FARGUHARDSON, 1970) and with numerical evaluations of co-tidal charts for the Scotian Shelf and the Grand Banks of Newfoundland (DE MARGERIE and LANK, 1986). Such an assumption also agrees with satellite observations that show internal waves propagating normally to the mean depth contours of the continental shelf (APEL and GONZALES, 1983).

The model in both cases is initialized without any bed features other than the mean slope that is estimated from measured bathymetry. The initial bed configuration for the Grand Banks of Newfoundland and Sable Island Bank are shown in Figs 2 and 3 together with the localization of the bed profiles that will be considered here. Figures 2 and 3 also contain stratification parameters which are: $h_1 = 30$ m; $h_2 = 50$ m; and $\rho = (\rho_2 - \rho_1)/\rho_2 = 0.00275$. These were chosen to agree with the data for the Scotian Shelf reported by SANDSTRÖM and ELLIOTT (1984) and SANDSTRÖM *et al.* (1989).

For the Grand Banks example the mean incident wave period, T, was chosen to be 750 s with a corresponding mean incident frequency $\omega_1 = 0.0189$ (SANDSTRÖM, personal communication). The incident wavelength, λ, of ζ is in this case 516 m at a water depth, $H = 80$ m.

For the calculations pertaining to Sable Island Bank the mean period of the train of internal oscillations was chosen to be $T = 1100$ s from which the mean incident frequency is $\omega_1 = (2\pi/T)(h_2/g)^{1/2} = 0.0129$. The incident wavelength of the interface displacement, ζ is obtained from the dispersion relation (5) and has the value $\lambda_1 = 800$ m at $H = 80$ m.

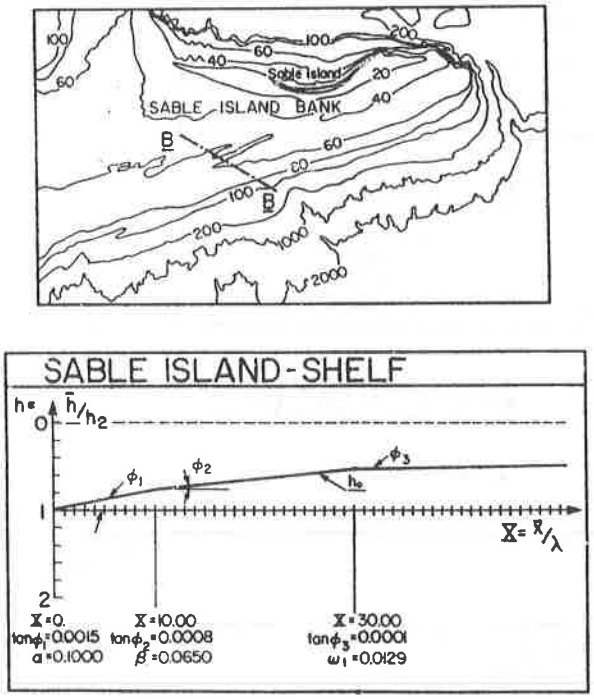

Fig. 3. A location diagram showing the initial seabed and incident wave and stratification parameters in the calculation for Sable Island Bank.

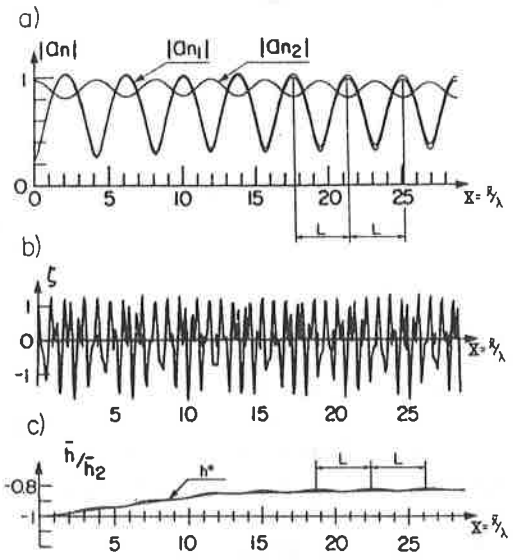

Fig. 4 Predicted sand ridge development for the Grand Banks of Newfoundland along the chosen transect with initial data shown in Fig. 2: (a) the Fourier-amplitudes $|a_1|$ and $|a_2|$ of the modal components of ζ; (b) an instantaneous interface ζ; and (c) the initial ($t = 0$) and final ($t = 1000\tau$) bed topography.

In both cases the incident internal waves are long in comparison to the incident water depth of the fluid layers. Consequently they may be viewed as long waves over the entire shelf. Thus the wave motion and the related bed deformation may in principle be described using our model.

The interface displacement is taken to be of finite amplitude and the parameter α is set to 0.10 at $X = 0$.

In our model calculations we took it that the waves were coming in continuously whereas in reality one only has a couple of wave packets each day. Moreover in the winter season, at both of the above sites, the stratification disappears and with it the internal wave climate. These aspects only serve to change the time scale over which the predicted bed forms come to equilibrium. For during periods when there is no large-scale motion the bottom sediment will remain undisturbed (AMOS and JUDGE, this issue). Of importance is the fact that we assume the existence of a repetitive process that generates these wave packets, and that the waves have relatively stable wavelengths, phases, and amplitudes. This appears to be the case in some locations (c.f. HOLLOWAY, 1987) and it has been taken as a working hypothesis here. A more realistic view would be to input a random wave that follows a chosen energy spectrum. We hope to give consideration to this prospect in the future.

Results of numerical experiments for the Grand Banks of Newfoundland are presented in Fig. 4a–c. The harmonic amplitudes $|a_1|$ and $|a_2|$ of the two modal components of the interface, ζ, are presented in Fig. 4a. The instantaneous wave profile over the final bed profile (at a time equal to 600 τ) is shown in Fig. 4b. The initial and final state of the bed topography is shown in Fig. 4d (these correspond to the initial time and 600τ time units later, respectively).

Table 1. *Sensitivity of the repetition length*, L, *to the incident wave period*, T

T (s)	750	900	1000	1020	1100
$\omega_1 = (2\pi/T)\sqrt{(h_2/g)}$	0.0189	0.0158	0.0142	0.0139	0.0129
k_1	0.6089	0.5025	0.4799	0.4412	0.4072
$\lambda_1 = (2\pi/k_1)h_2$ (m)	503	625	664	712	850
$L = \bar{L}/\lambda_1$	4.20	4.45	4.75	5.00	5.65
$\bar{L}$ (m)	2012	2781	3154	3560	4800

Qualitative description of the model's behaviour

The most important aspect of the evolution of the model's waves, seen transparently in the evolution of the interface, ζ, is a slow modulation of the first and second harmonics and a mean increase in the energy of the second harmonic due to shoaling. Energy is exchanged between the modal wave components in a nearly periodic fashion. The horizontal distance between two successive minima of the second harmonic amplitude $|a_2|$ is referred to as the *local repetition length*, L. Our earlier work showed that the repetition length is also a typical parameter characterizing the propagation of nonlinear, surface gravity waves in shallow water (BOCZAR-KARAKIEWICZ *et al.*, 1987). Such an energy transfer towards higher harmonics in internal waves has been observed in laboratory experiments with regular waves (WALLACE and WILKINSON, 1988) and in spectra of internal waves propagating over continental shelves (HALL and PAO, 1969).

The repetition length is typically several times the length associated to the interfacial oscillations. It is also a characteristic length scale in the pattern of the associated velocity field and consequently in the scale of the sediment flux pattern, Q_m. The continuity described by equation (11) relates to the divergence of the spatially oscillating sediment flux with instantaneous changes in the bed configuration, $h(X)$. Thus the repetition length determines the spacing of the sand ridges that evolve from the initially featureless bed topography, shown in Fig. 4c (erosion occurs forming the troughs of the sand ridges where $\partial Q_m/\partial X$ is positive, while sand ridge crests are formed where $\partial Q_m/\partial X$ is negative).

Quantitative predictions and comparisons with field data

For this study we considered the most important output of the model to be the repetition length as this determines to a considerable degree the location and spacing of the sand ridges. The crucial input parameters in the model about whose values there may be doubt are the incoming internal-wave frequency, ω_1, the best choice of the relative water depths h_1 and h_2 to model the existing oceanic environment, and the total water depth. The stratification parameter, ρ, appears to vary only slightly from site to site (see SANDSTRÖM and ELLIOTT, 1984; and compare with HOLLOWAY, 1987). Moreover a change in ρ by a multiplicative factor, γ, is equivalent in the model to dividing ω_1 by the square root of γ. The dependence of the repetition length on the amplitude parameter, α, was found to be quite weak compared with its dependence on other parameters.

Tables 1, 2 and 3 contain typical results generated in our study. Table 1 shows the model's sensitivity to the incident wave period, T, with the total depth, H, fixed at 80 m, the incident internal wave period at 1100 s, the amplitude parameters, α, at 0.1, and the

Table 2. Sensitivity of the repetition length L, *to the total depth*, H

H (m)	80	160
ω_1	0.0129	0.0200
k_1	0.4072	0.7861
λ_1 (m)	850	959
L	5.65	3.85
L (m)	4800	3597

density parameter $\rho = (\rho_2 - \rho_1)/\rho_1$ at 0.00275. Table 2 gives an indication of the independence of the repetition length on the total water depth with the upper layer depth, h_1, fixed at 30 m, the incident wave period at 1100 s, the density parameter, ρ, at 0.00275, and α still set to 0.1. In Table 3 the repetition length is determined for different geometries of stratification. The total depth, H, is fixed at 80 m, the upper layer depth is 30 m, the density parameter is 0.00275, and α is set to 0.1. In the tables, L is the repetition length in wavelengths predicted by the model while $\bar{L}$ is the physical value of the repetition length. The wavenumber, k_1, is computed from ω_1 using the dispersion relation (5).

The repetition length is seen to depend fairly strongly on both the incoming internal-wave period and the stratified structure but less substantially on total water depth. In consequence caution should be observed in interpreting the model predictions.

Comparison of observed and predicted topographies (Fig. 5a) show reasonable agreement in the spacing of ridge crests. However observed sand-ridge morphology is more complex than the predictions made on the basis of our model and sand ridges are higher than predicted. In Fig. 5b the instantaneous profile of the interface is shown over a distance of one repetition length. A comparison of the prediction of ζ shows surprising similarities with observed nonlinearities in time series of wave-induced currents (HOLLOWAY, 1987).

Figure 6a and b show results of a similar calculation performed for a bed profile on Sable Island Bank. Observations reported in Fig. 6a show the spacing of sand ridges to be some 6000 m (at a water depth of 70 m), whereas distances predicted by the model are about 5000 m as depicted in Fig. 6b. Considering the uncertainties in the data this level of agreement is encouraging.

The results presented for the Grand Banks of Newfoundland and Sable Island Bank (Figs 5a and 6b) indicate that the sand-ridge morphology is affected strongly by the initial mean slope of the continental shelf. Another numerical experiment has been performed

Table 3. Sensitivity of the repetition length, L, *to the geometry of the stratification*

h_1 (m)	30	40	50
h_2 (m)	50	40	30
ω_1	0.0129	0.0155	0.0168
λ_1 (m)	850	620	585
L	5.00	4.44	4.37
$\bar{L}$ (m)	4800	2653	2476

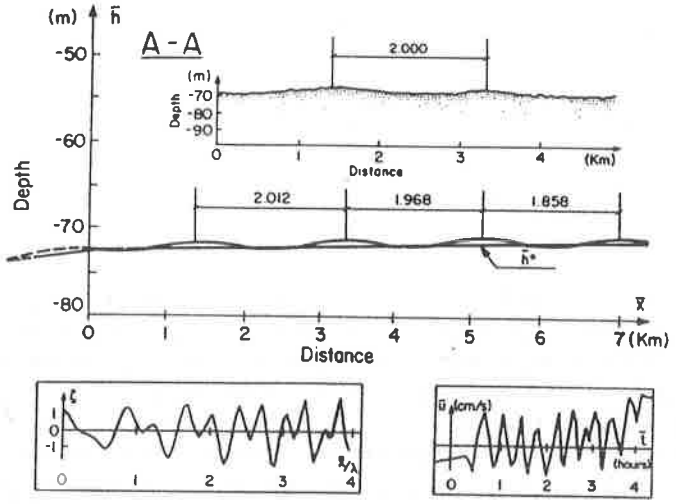

Fig. 5. (a) A comparison between the measured and predicted sand-ridge topographies for the Grand Banks of Newfoundland (see Fig. 2); (b) typical, predicted, instantaneous profile of the interface ζ, and an example of an observed time series of the wave-induced currents at a location in which the total water depth is 120 m (after HOLLOWAY, 1987)

simulating the formation of sand ridges on a relatively steep continental slope (the mean gradient applied in this calculation was 0.01). Such is the case on continental shelves of southeastern Australia (FIELD and ROY, 1984) and in southeastern Africa (MARTIN and FLEMING, 1986). In this evaluation the stratification and incident wave parameters as used in the Sable Island calculations were applied. Results are presented in Fig. 7. Comparisons show that fewer crests appear over a given change in water depth and the crest-to-crest distance decreases when the mean slope is increased. The strong influence of seabed on sand-ridge topography is generally confirmed by observations. In the case of steep continental shelves only one or two ridges are observed as shown in our predictions (Fig. 7). With decreasing slope (Sable Island Bank) the number of sand ridges increases. The

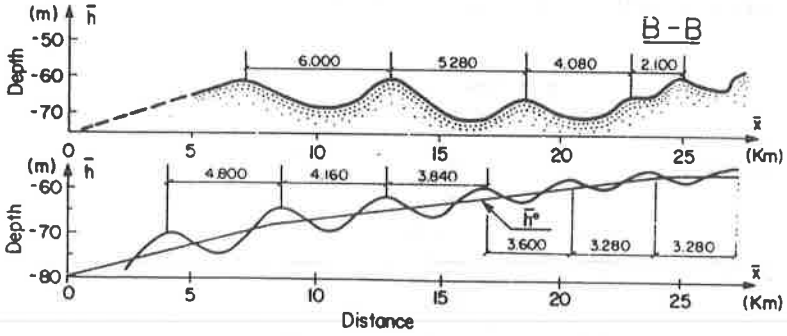

Fig. 6. Sand ridge development for Sable Island Bank (south) along the chosen transect with the initial data presented in Fig. 3: (a) the actual measured bed profile; and (b) the initial featureless bed ($t = 0$) and the predicted final bed topography ($t = 600\tau$).

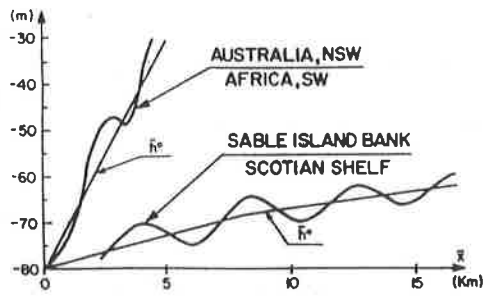

Fig. 7. Model predictions of sand ridge topographies on continental shelves showing the slope and depth-control of crest-to-crest distances and of the number of crests in a sand-ridge system. The vertical axis, z, indicates the water depth in metres; horizontal distances are measured in kilometres.

limiting configuration is a semi-infinite horizontal seabed where there will be no limit to the number of sand-ridge crests.

The present model predicts a continuous and gradual offshore-directed flux of sediment. However the applicability of the presented model is restricted to those parts of the continental shelf where the local depth of the lower layers, $\bar{h}(\bar{x})$, is larger than the thickness, h_1, of the upper layer, $\bar{h}(\bar{x}) \geq h_1$. In shallower parts of the continental shelf where $\bar{h}(\bar{x}) < h_1$ a more accurate description of the internal oscillation is necessary. A cubic term neglected in our model has to be taken into account (GEAR and GRIMSHAW, 1983; HELFRICH and MELVILLE, 1986) in order to describe the change of polarity in the internal oscillations. Such a change of polarity may occur when $\bar{h} \simeq h_1$, and this change is associated with an inversion of the net, near-bed sediment flux to a shoreward direction. Based on the stratification parameters applied in our calculations such a situation would occur at a waterdepth of approximately 60–50 m.

In a stable stratified water column the propagation of internal oscillations would continue in the shoreward direction until $h(x)$ approaches zero at which point the internal oscillation would break down. Laboratory experiments indicate that the process of propagation, sloping and breaking of internal waves show many similarities to that of surface waves (WALLACE and WILKINSON, 1988; SOUTHARD and CACCHIONE, 1972). In the breaking region the interaction one observes is the formation of bar-like sediment structures. Stratification is no longer maintained past the breaking region and wave-bed interactions due to internal waves ceases.

CONCLUSIONS

A mechanism has been proposed for the formation of large-scale sand ridges by internal waves having periods of order 15–20 min. Comparisons are made between predictions of a mathematical model incorporating this mechanism and field data from the Grand Banks of Newfoundland and Sable Island Bank.

The following conclusions are derived from these comparisons:

(1) Despite the lack of free parameters with which data can be fit, the model predicts actual crest-to-crest distances of measured sand ridges reasonably well.

(2) According to the model the horizontal distances between adjacent ridge crests are on the order of kilometres and they are several times the mean, local wavelength of the assumed incident train of internal waves. This is also consistent with observations.

(3) Crest-to-crest distances predicted by the model are depth and slope dependent. They increase gradually with increasing depth. Also the number of crests and their separation increase with decreasing slope.

(4) The long term sediment flux resulting from internal waves is predicted to be offshore.

(5) A quantitative analysis of the wave-bottom interaction in the shallower part of the shelf indicates the potential for an inversion resulting in a net, shoreward, sediment flux.

(6) It is suggested that internal-wave breaking and the resulting mixing cuts off the effects of stratification and, consequently the propagation of coherent internal oscillations in the coastal region.

Acknowledgements—Support for this project was provided by the Government of Canada, the Ministry of Energy, Mines and Resources (Grant 276188), the Natural Sciences and Engineering Research Council of Canada (Grant 0GP0002621) and the United States National Science Foundation. Valuable assistance and commentary was provided by Professor R. Grimshaw and Dr Peter Holloway (University of N.S.W., Australia), Dr P. Roy, Professor B. Thom and Dr M. A. Ferland (University of Sydney, Australia).

REFERENCES

AMOS C. L. and J. T. JUDGE (this issue) Sediment transport on the eastern Canadian continental shelf. *Continental Shelf Research*, **11**, 1069–1082.

AMOS C. L. and E. L. KING (1984) Bedforms of the Canadian Eastern Seaboard: a comparison with global occurrences. *Marine Geology*, **57**, 167–208.

AMOS C. L. and O. C. NADEAU (1988) Surficial sediments of the outer banks, Scotian Shelf, Canada. *Canadian Journal of Earth Sciences*, **25** (12), 1923–1944.

AMOS C. L., A. J. BOWEN, D. A. HUNTLEY and J. T. JUDGE (1988) Bedorm stability under waves and currents. In: *Proceedings of workshop on roughness and friction*, D. H. WILLIS and B. GREEWOOD, editors, National Research Council Canada, Ottawa, pp. 62–74.

APEL J. R. (1979) Observations of internal-wave surface signatures in ASTP photographs. In: *Apollo-Soyuz test project*, Summary Science Report, NASA, SP-H12, pp. 505–509.

APEL J. R. (1980) Satellite sensing of ocean surface dynamics. *Annual Review of Earth and Planetary Sciences*, **8**, 303–342.

APEL J. R. and F. I. GONZALES (1983) Nonlinear features of internal waves off Baja California as observed from the Seasat imaging radar. *Journal of Geophysical Research*, **88**, (C7), 4459–4466.

APEL J. R., H. M. BYRNE, J. R. PRONI and R. L. CHARNELL (1975) Observations of oceanic internal and surface waves from the Earth resources technology satellite. *Journal of Geophysical Research*, **80**, 865–881.

BAINES P. G. (1981) Satellite observations of internal waves on the Australian North-West Shelf. *Australian Journal of Marine and Freshwater Research*, **32**, 457–463.

BARRIE, J. V., C. F. M. LEWIS, G. B. FADER and L. H. KING (1984) Seabed processes on the northeastern Grand Banks of Newfoundland; modern reworking of relict sediments. *Marine Geology*, **57**, 209–227.

BENNEY D. J. (1966) Long non-linear waves in fluid flows. *Journal of Mathematical Physics* **45**, 52–63.

BOCZAR-KARAKIEWICZ B. and J. L. BONA (1986) Wave-dominated shelves: A model of sand ridge formation by progressive infragravity waves. In: *Shelf sand and sandstones*, J. KNIGHT and J. R. MCLEAN, editors, Canadian Society of Petroleum Geologists, Memoir II, pp. 163–179.

BOCZAR-KARAKIEWICZ B., J. L. BONA and D. L. COHEN (1987) *Interaction of shallow-water waves and bottom topographies*. Proceedings of the Workshop on Dynamical Problems in Continuum Physics held at the Institute of Mathematics and its Applications, The University of Minnesota, Minneapolis, June 1985, Springer-Verlag, New York, pp. 131–176.

BOCZAR-KARAKIEWICZ B., C. L. AMOS and G. DRAPEAU (1991) The origin and stability of sand ridges on Sable Island Bank, Scotian Shelf. *Continental Shelf Research*, in press.

CHAPALAIN G. (1988) Étude hydrodynamique et sedimentaire des environnements littoraux dominés par la houle. Ph.D. Thesis, Université de Grenoble, Institut de Mécanique de Grenoble, France, pp. 318.

CHAPALAIN G. and B. BOCZAR-KARAKIEWICZ (1989) *Longshore bar formation in coastal wave-dominated areas*. Proceedings of Technical Session C, Maritime Hydronamics, XXIII Congress Int. Ass. Hydr. Res. held in Ottawa in August, 1989. National Research Council, Canada, pp. 531–538.

CHAPALAIN G. and B. BOCZAR-KARAKIEWICZ (1991) Hydrodynamics and sedimentary processes induced by water waves and the formation of longshore bars Part I: Basic concepts in the case of uniform sediment, Part II: A model with non-uniform sediment, in preparation.

CACCHIONE D. A. and J. B. SOUTHARD (1974) Incipient sediment movement by shoaling internal gravity waves. *Journal of Geophysical Research*, **70**, 2237–2242.

DE MARGERIE S. and K. D. LANK (1986) *Tidal circulation of the Scotian Shelf and Grand Banks*. ASA Consulting Ltd., Dartmouth, N.S., Canada, p. 18.

DJORDJEVIC V. D. and L. G. REDEKOPP (1978) The fission and disintegration of internal solitary waves moving over two-dimensional topography. *Journal of Physical Oceanography*, **8**, 1016–1024.

DUANE D. B., M. E. FIELD, E. P. MEISBURGER, D. J. P. SWIFT and S. J. WILLIAMS (1972) Linear shoals on the Atlantic inner continental shelf, Florida to Long Island. In: *Shelf sediment transport—process and pattern*, D. J. P. SWIFT, D. B. DUANE and O. H. PILKEY, editors, Dowden, Hutchinson and Ross Inc., Stroudsburg, PA, pp. 447–498.

FADER G. B. and L. H. KING (1981) *A reconnaissance study of the surficial geology of the Grand Banks of Newfoundland*. Current Research, Part A, Geological Survey of Canada, Paper 81–14, pp. 45–56.

FARGUHARDSON W. I. (1970) Tides, tidal streams and currents in the Gulf of St. Lawrence. AOL. Report, Bedford Institute 1970–1975, unpublished manuscript.

FIELD M. E. (1980) Sand bodies on coastal plain shelves: Holocene record of the U.S. Atlantic inner shelf off Maryland. *Journal of Sedimentary Petrology*, **50** (2), 505–528.

FIELD M. E. and P. S. ROY (1984) Offshore transport and sand-body formation: evidence from a steep, high-energy shoreface, Southeastern Australia. *Journal of Sedimentary Petrology*, **54** (4), 1292–1302.

GEAR J. A. and R. GRIMSHAW (1983) A second-order theory for solitary waves in shallow fluids. *Physical Fluids*, **26** (1), 14–29.

HALL J. M. and Y-H. PAO (1969) Spectra of internal waves in stratified fluids. Part 2. *Radio Science*, **11**, 1321–1325.

HEATHERSHAW A. D., A. L. NEW and P. D. EDWARDS (1987) Internal tides and sediment transport at the shelf break in the Celtic Sea. *Continental Shelf Research*, **7** (5), 485–517.

HELFRICH K. R., W. K. MELVILLE and J. W. MILES (1984) On interfacial solitary waves over slowly varying topography. *Journal of Fluid Mechanics*, **149**, 305–317.

HELFRICH K. R. and W. K. MELVILLE (1986) On long nonlinear internal waves over slope-shelf topography. *Journal of Fluid Mechanics*, **167**, 285–308.

HOLLOWAY P. (1987) Internal hydraulic jumps and solitons at a shelf break region on the Australian North West Shelf. *Journal of Geophysical Research*, **92** (C5), 5405–5416.

HOOGENDOORN E. L. and R. W. DALRYMPLE (1986) Morphology, lateral migration and internal structures of shoreface-connected ridges, Sable Island Bank, Nova Scotia, Canada. *Geology*, **14**, 400–403.

HUNT J. N. (1954) The turbulent transport of suspended sediment in open channels. *Philosophical Transactions of the Royal Society, London*, **A246**, 322–335.

HUTHNANCE J. M. (1982) On one mechanism forming linear sand banks. *Estuarine, Coastal and Marine Science*, **14**, 79–99.

IVEY G. N. and R. Y. NOKES (1989) Vertical mixing due to the breaking of critical internal waves on sloping boundaries. *Journal of Fluid Mechanics*, **204**, 479–500.

JACOBS S. J. (1984) Mass transport in a turbulent boundary layer under a progressive water wave. *Journal of Fluid Mechanics*, **146**, 303–312.

JOHNS B. (1970) On the mass transport induced by oscillatory flow in a turbulent boundary layer. *Journal of Fluid Mechanics*, **43**, 177–185.

KAO T. W., FUH-SHING PAN and D. RENOUARD (1985) Internal solitons on the pycnocline: generation, propagation, and shoaling and breaking over a slope. *Journal of Fluid Mechanics*, **159**, 19–53.

KARL H. A., D. A. CACCHIONE and P. R. CARLSON (1986) Internal-wave currents as a mechanism to account for large sand waves in Navarinsky Canyon Head, Bering Sea. *Journal of Sedimentary Petrology*, **56** (5), 706–714.

KELLER J. B. (1988) Resonantly interacting water waves. *Journal of Fluid Mechanics*, **191**, 529–534.

Kinsman B. (1965) *Wind waves: their generation and propagation on the ocean surface*. Prentice Hall, Englewood Cliffs, New Jersey, 676 pp.
Longuet-Higgins M. S. (1953) Mass transport in water waves. Philosophical Transactions of the Royal Society, London, A **245**, 535–581.
Mahony J. J. and W. G. Pritchard (1980) Wave reflection from beaches. *Journal of Fluid Mechanics*, **101**, 809–832.
Martin A. K. and B. W. Flemming (1986) The holocene shelf sediment wedge off the South and East coast of South Africa. In: *Shelf sands and sandstones*, R. J. Knight and J. R. McLean, editors. Can. Soc. Petr. Geol., Memoir II, pp. 27–44.
Maxworthy T. (1979) A note on the internal solitary waves produced by tidal flow over a three-dimensional ridge. *Journal of Geophysical Research*, **84**, 338–346.
Nielsen P. (1988) Three simple models of wave sediment transport. *Coastal Engineering*, **12**, 43–62.
Richards K. J. (1980) The formation of ripples and dunes on an erodible bed. *Journal of Fluid Mechanics*, **99**, 597–618.
Sandström H. and J. A. Elliott (1984) Internal tide and solitons on the Scotian Shelf: a nutrient pump at work. *Journal of Geophysical Research*, **89** (C4), 6415–6426.
Sandström H., J. A. Elliott and N. A. Cochrane (1989) Observing groups of solitary internal waves and turbulence with BATFISH and echo-sounder. *Journal of Physical Oceanography*, **19**, 987–997.
Smyth J. F. and P. E. Holloway (1988) Hydraulic jump and undular bore formation on a shelf break. *Journal of Physical Oceanography*, **18** (7), 947–962.
Southard J. B. and D. A. Cacchione (1972) Experiments on bottom sediment movement by breaking internal waves. In: *Shelf sediment transport: process and pattern*, D. J. P. Swift, B. B. Duane and O. H. Pilkey, editors, Dowden, Hutchinson and Ross, Stroudsbourg, PA, pp. 83–97.
Stewart P. L. (1986) SLAR and sounders spot solitons. *Offshore Resources*, **4**, 19.
Swift D. J. P. and G. L. Freeland (1978) Current lineations and sand waves on the inner shelf. Middle Atlantic Bight of North America. *Journal of Sedimentary Petrology*, **48** (4), 1257–1266.
Swift D. J. P., J. W. Kofoed, F. P. Saulsbury and P. Sears (1972) Holocene evolution of the shelf surface, Central and South Atlantic shelf of North America. In: *Shelf sediment transport: process and pattern*, D. J. P. Swift, D. B. Duane and O. H. Pilkey, editors, Dowden, Hutchinson and Ross Inc., Stroudsbourg, PA, pp. 499–574.
Turner J. S. (1973) *Buoyancy effects in fluids*. Cambridge University Press, 367 pp.
Villaret C. and Y. P. Sheng (1988) *Modelling stratified turbulent boundary layers*. Proceedings of the International Conference on Coastal Engineering, ASCE., Spain, pp. 321–332.
Wallace B. C. and D. L. Wilkinson (1988) Run-up of internal waves on a gentle slope in a two-layer system. *Journal of Fluid Mechanics*, **191**, 419–462.

APPENDIX

Model equations for internal oscillations in a two-layer system: definition of functions G *and* G_j, *and of coefficients* A_j, B_j (j = 1, 2), C *and* D

The first-order evolution equation for the interface $\zeta = \zeta^{(1)}$ derived from (1.1–1.5) is

$$\zeta^{(1)}_{tt} - \frac{h_1}{H}\rho\zeta^{(1)}_{xx} - \frac{1}{3}\frac{H}{h_2}\zeta^{(1)}_{xxtt} = 0. \tag{A.1}$$

The second-order evolution equation for $\zeta^{(2)}$ reads

$$\zeta^{(2)}_{tt} - \frac{h_1}{H}\rho\zeta^{(2)}_{xx} - \frac{1}{3}\frac{H}{h_2}\zeta^{(2)}_{xxtt} = G(\zeta^{(1)}, \frac{h_2}{h_1}, h, \rho). \tag{A.2}$$

For a modally-decomposed interface $\zeta = \zeta(X, x, t)$ as in (3), the right-hand side of (A.2) may be presented in the series

$$G(X, x, t) = \sum_{j=1}^{2} e^{i\omega_j t} G_j(X, x) + * + \cdots, \tag{A.3}$$

The function $f(X)$ describing the bed topography $z = -h(X)$ may also be Fourier-decomposed in the form

$$f(X) = \sum_{-\infty}^{+\infty} f_n(X) e^{ink_1 x}. \tag{A.4}$$

Substituting ζ from (3) and $f(X)$ from (A.4) into the right-hand side of (A.2), we obtain the following solvability conditions for the finite-amplitude second approximation (A.2)

$$\frac{k_1}{2\pi}\int_0^{2\pi/k_1} e^{\pm ik_1 x} G_1(X, x)\, dx = 0 \tag{A.5}$$

$$\frac{k_2}{2\pi}\int_0^{2\pi/k_2} e^{\pm i2k_2 x} G_2(X, x)\, dx = 0 \tag{A.6}$$

where G_1 and G_2 are as in (A.3).

The solvability conditions (A.5) and (A.6) lead to the model equations (6) for the modal amplitudes of ζ. The coefficients of these equations are given by following the expression: for $j = 1, 2$

$$H_j = \frac{A_j}{B_j}, \quad \text{and} \quad S_1 = \frac{C}{B_1}, \quad S_2 = \frac{D}{B_2},$$

$$A_j = \tfrac{1}{2}\omega_j^2(1 - \tfrac{1}{3}k_j^2),$$

$$B_j = \rho k_j^2\left[1 - \frac{1}{6\rho}\frac{H}{h_2}\omega_j^2\right],$$

$$C = \frac{3}{2}\omega_1^2\left[1 - \left\{\frac{h_2}{h_1}\right\}^2 + \left\{\frac{4k_1}{3}\right\}^2\right],$$

$$D = -\frac{3}{4}\omega_1^2\frac{k_2 - k_1}{k_1}\left[1 - \left\{\frac{h_2}{h_1}\right\}^2 + \frac{2}{9}\frac{k_2 + 2k_1}{k_2}(k_2 - k_1)^2\right].$$